This is a non-peer reviewed preprint submitted to EarthArXiv and under review in Geophysical J.Int.

A proxy implementation of thermal pressurization for earthquake cycle modeling on rate-and-state faults

Marco T. Herrera[1,2], J. P. Ampuero[3], Jorge G. F. Crempien[1,2]

[1]Department of Structural and Geotechnical Engineering, Pontificia Universidad Católica de Chile, Santiago, Chile.

[2]National Research Center for Integrated Natural Disaster Management (CIGIDEN), Chile.

[3]Université Côte d'Azur, IRD, CNRS, Observatoire de la Côte d'Azur, Géoazur, Valbonne, France.

Corresponding author: Marco T. Herrera (mtherrera2@uc.cl) / +51995502664

This is a non-peer reviewed preprint submitted to EarthArXiv and under review in Geophysical J.Int.

Summary

The reduction of effective normal stress during earthquake slip due to thermal pressurization of fault pore fluids is a significant fault weakening mechanism. Explicit incorporation of this process into frictional fault models involves solving the diffusion equations for fluid pressure and temperature outside the fault at each time step, which significantly increases the computational complexity. Here, we propose a proxy for thermal pressurization implemented through a modification of the rate-and-state friction law. This approach is designed to emulate the fault weakening and the relationship between fracture energy and slip resulting from thermal pressurization and is appropriate for fully-dynamic simulations of multiple earthquake cycles. It preserves the computational efficiency of conventional rate-and-state friction models, which in turn can enable systematic studies to advance our understanding of the effects of fault weakening on earthquake mechanics. In 2.5D simulations of pulse-like ruptures on faults with finite seismogenic depth, we find that the spatial distribution of slip velocity near the rupture front is consistent with the conventional square-root singularity, despite continued slip-weakening within the pulse, once the rupture has propagated a distance larger than the rupture width. An unconventional singularity appears only at shorter rupture distances. We further derive and validate numerically a theoretical estimate of the fracture energy dissipated by thermal pressurization in earthquake cycles. These results support the use of fracture mechanics theory to understand the propagation and arrest of very large earthquakes.

Keywords

Subduction zone processes; Friction; Earthquake dynamics; Numerical modelling.

1 Introduction

Understanding how faults lose their strength during rapid earthquake slip is important for constraining the minimum level of stress a fault requires to rupture catastrophically, which can help improve earthquake hazard assessment and prediction (Viesca and Garagash, 2015; Noda and Lapusta, 2013; Tinti et al., 2005; Abercrombie and Rice, 2005; Perry et al., 2020).

Earthquake models with enhanced dynamic weakening have been successful in reproducing fault operation at low apparent strength (low average ratio of shear stress to normal stress) and low heat production, as supported by several observations (Thomas et al., 2014; Viesca and Garagash, 2015; Perry et al., 2020; Lambert and Lapusta, 2023). Two important mechanisms for dramatic fault weakening incorporated in such models are the reduction of the friction coefficient due to flash heating of micro-contacts of rough fault surfaces or gouge (Viesca and Garagash, 2015; Goldsby and Tullis, 2011; Mase and Smith, 1987; Noda et al., 2011) and the reduction of the effective normal stress by the thermal pressurization (TP) of fault zone pore fluids (Viesca and Garagash, 2015; Garagash, 2012; Noda and Lapusta, 2013; Perry et al., 2020; Rempel and Rice, 2006).

TP occurs when frictional heating on a principal slip zone causes the pore fluid in the surrounding gouge to tend to thermally expand, leading to increase in fluid pressure, reduction in effective normal stress and thus reduction in fault strength (Viesca and Garagash, 2015; Garagash, 2012; Noda and Lapusta, 2013; Perry et al., 2020; Rempel and Rice, 2006). As shown by Viesca and Garagash (2015), TP can account for important aspects of the scaling of fracture energy with slip inferred from seismological observations over seven orders of fault slip magnitude, spanning small to large earthquakes. This suggests that TP is a widespread and prominent process for fault weakening.

Models with enhanced dynamic weakening due to TP can explain both the increasing trend in breakdown energy with increasing event size and the near magnitude-invariance of stress drops (Viesca and Garagash, 2015; Perry et al., 2020). As shown in Figure 1, the widely used rate-and-state (Dieterich, 1978, 1979; Ruina, 1983) and linear slip-weakening (Andrews, 1976; Ida, 1972) friction models have a distinct residual strength and produce a fracture energy G_c that does not depend on slip D. In contrast, models that account for thermal pressurization on the fault feature continued slip-weakening, leading to $G_c \propto D^{2/3}$ in the diffusion-dominated regime at large slip and $G_c \propto D^2$ in the undrained-adiabatic regime at small slip $\ll 0.1$ m (Viesca and

Garagash, 2015).

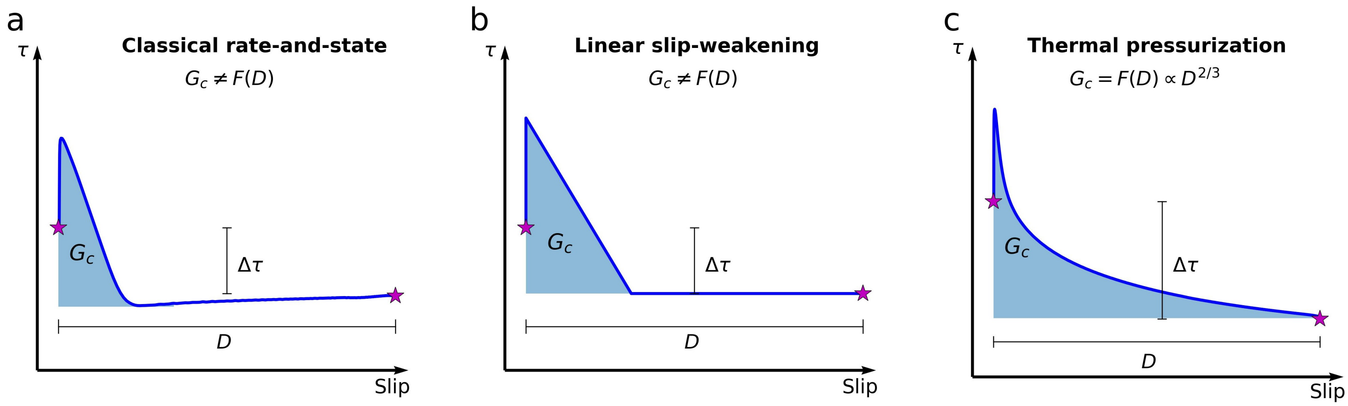

Figure 1: Slip-weakening curves and fracture energy G_c for a) classical rate-and-state friction, b) linear slip weakening friction, and c) thermal pressurization weakening in the diffusion-dominated regime. Stars indicate the initial and final states of an earthquake. Final slip D and stress drop $\Delta\tau$ are indicated.

The behavior of rate-and-state faults with enhanced weakening has been widely studied through numerical simulation of sequences of earthquake cycles (Perry et al., 2020; Noda and Lapusta, 2013; Noda et al., 2011; Thomas et al., 2014). Implementing flash-heating in an earthquake simulator only requires modifying the friction law. In contrast, incorporating thermal pressurization requires solving the diffusion equations for fluid pressure and temperature within the fault zone (in the direction normal to the fault surface) coupled to fault slip (Noda and Lapusta, 2013; Perry et al., 2020; Mavrommatis et al., 2017). This implies a higher computational cost and complexity, which limits the capacity to conduct large sets of simulations, especially with realistically large values of the ratio between fault size and the along-fault length scales arising from friction and TP.

Therefore, in Section 2 we propose a TP proxy implementation through a modification of the rate-and-state friction law, amenable for convenient computational implementation, having low computational cost, and designed to mimic the fault weakening and scaling between fracture energy and slip that emerge from TP. We incorporate the thermal weakening effect via the friction coefficient and keep the effective normal stress constant in time. The proposed proxy implementation has similar complexity and computational cost as conventional rate-and-state friction.

In Section 3, we present examples of results of earthquake cycle simulations with the TP proxy and flash heating implemented in a fully-dynamic 2.5D earthquake cycle simulator, which accounts for the effect of a finite seismogenic width W. We show that the asymptotic behavior of slip rate, as a function of distance behind the rupture front, supports the applicability of fracture mechanics theory to very large earthquakes with rupture lengths $> W$ despite continued weakening by TP. To enable such fracture mechanics analyses, in Section 4 we derive and validate theoretical estimates of the fracture energy produced by the TP proxy in earthquake cycle simulations.

2 Thermal pressurization proxy

2.1 Rate-and-state friction law

We take as starting point the formulation of rate-and-state friction (Dieterich, 1978, 1979; Rice and Ruina, 1983; Ruina, 1983) with flash heating used by (Harris et al., 2018; Noda et al., 2011; Thomas et al., 2014). That formulation is summarized in this section.

The shear stress τ on the fault satisfies

$$\tau = \sigma f(V, \Psi) \tag{1}$$

where σ is the effective normal stress on the fault and f the friction coefficient. The latter depends on slip velocity V and a fault state variable Ψ as

$$f(V, \Psi) = a \ \mathrm{arcsinh}\left(\frac{V}{2V_0} \exp\frac{\Psi}{a}\right) \tag{2}$$

where a is a rate-and-state parameter and V_0 a reference velocity. This is a regularized version of the classical rate-and-state law, designed to prevent a singularity at zero velocity (Ben-Zion and

Rice, 1997; Lapusta et al., 2000). We consider the slip-law for the state evolution:

$$\dot{\Psi} = -\frac{V}{L}(\Psi - \Psi_{ss}(V)) \tag{3}$$

where

$$\Psi_{ss}(V) = f_0 + b \log \frac{V_0}{V} \tag{4}$$

L is a characteristic slip distance, f_0 a reference friction coefficient and b a rate-and-state parameter. Equations 1-4 completely define the frictional fault strength.

The state variable Ψ is a re-formulation of the classical rate-and-state state variable θ. They are related by

$$\Psi = f_0 + b \log \frac{V_0 \theta}{L} \tag{5}$$

This re-formulation is computational advantageous: it improves the stability of the numerical friction solver.

At steady state, when $\dot{\Psi} = 0$, the state variable Ψ is equal to $\Psi_{ss}(V)$ and the friction coefficient is

$$f_{ss}(V) = a \text{ arsinh} \left(\frac{V}{2V_0} \exp \frac{\Psi_{ss}(V)}{a} \right) \tag{6}$$

The corresponding classical state variable at steady state is $\theta_{ss} = L/V$.

2.2 Rate-and-state friction law with flash heating

The abrupt velocity-dependent reduction of the friction coefficient due to flash heating is introduced by re-defining the steady-state friction as

$$f_{ss}^{FH}(V) = \frac{f_{ss}(V) - f_w}{1 + \frac{V}{V_w}} + f_w, \tag{7}$$

where f_w is the residual friction coefficient and V_w the threshold velocity for the activation of flash heating. The steady-state values of friction and state variable including flash heating are related by an equation analogous to Eq. 6:

$$f_{ss}^{FH}(V) = a \text{ arsinh}\left(\frac{V}{2V_0} \exp \frac{\Psi_{ss}^{FH}(V)}{a}\right) \tag{8}$$

Equating Eqs. 7 and 8, we obtain an expression for $\Psi_{ss}^{FH}(V)$, which we then use in the state evolution law as

$$\dot{\Psi} = -\frac{V}{L}(\Psi - \Psi_{ss}^{FH}(V)) \tag{9}$$

The frictional fault strength including flash heating is completely defined by Equations 1, 2 and 7-9.

2.3 Rate-and-state friction law with TP proxy

To implement a thermal pressurization proxy, we introduce a new friction coefficient under steady-state conditions, denoted as f_{ss}^{TP}. To maintain simplicity, we implement the concept of strong weakening by modifying the friction coefficient rather than by modifying the effective normal stress σ. This approach facilitates the derivation of a scaling relationship between G_c and slip, following the approach outlined by Viesca and Garagash (2015). Our objective is not to fully replicate the intricate physics of thermal pressurization, but rather to satisfy the scaling relationship.

Here, we define a new state variable ϕ that approximates the slip only in the co-seismic phase. Following the procedure shown in Beeler et al. (2008), we design the evolution of ϕ to meet two physical constraints. During earthquakes, ϕ should increase with co-seismic slip, thus

$$\dot{\phi} \approx V \tag{10}$$

During inter-seismic phases, ϕ should reset to zero, thus

$$\dot{\phi} \approx -\phi/T^* \tag{11}$$

where T^* is a characteristic time scale for the state variable to return to zero after the co-seismic phase. We set that value at 0.1 s, shorter than the typical rise time of large earthquakes. We define the ϕ evolution equation as a weighted sum of both expressions:

$$\dot{\phi} = \Gamma V - (1-\Gamma)\frac{\phi}{T^*} \tag{12}$$

The weight $\Gamma(V)$ applies smoothly a velocity threshold V_{th} that separates inter-seismic and co-seismic effects:

$$\Gamma(V) = \frac{1}{1+\exp\left(-40\left(\frac{V}{V_{th}}-1\right)\right)} \tag{13}$$

We are interested here in modeling large earthquake that have large slip > 0.1 m. Following Viesca and Garagash (2015), the relevant TP regime at large slip is the diffusion-dominated regime, in which the fracture energy G_c scales with co-seismic slip δ as $G_c \propto \delta^{2/3}$. As G_c results from the integral of the fault shear stress τ (Figure1c), then τ should be reduced by a factor $\propto \delta^{-1/3}$. In our proxy implementation, ϕ tends to δ during earthquakes, we keep σ constant and modify the steady-state friction as:

$$f_{ss}^{TP}(V,\phi) = \frac{f_{ss}(V)}{(1+\frac{\phi}{L^*})^{1/3}}, \tag{14}$$

where L^* is a characteristic slip distance for thermal pressurization (Rice, 2006; Rempel and Rice, 2006):

$$L^* = \left(\frac{2\rho c}{f\Lambda}\right)^2 \frac{(\sqrt{\alpha_{hy}}+\sqrt{\alpha_{th}})^2}{V_*}, \tag{15}$$

with ρc the specific heat, α_{hy} the hydraulic diffusivity, α_{th} the thermal diffusivity, f the friction coefficient prior the thermal pressurization, V_* a characteristic elastodynamic slip rate $\sim f\sigma c_s/\mu$, with c_s as the shear wave speed; and Λ the thermal pressurization coefficient relating increments of pore fluid pressure to increments in temperature.

Note that in Eq. 14, the state variable ϕ is not necessarily at steady state. Nonetheless, for historical reason and simplicity, we keep the terminology f_{ss}^{TP}. The steady-state friction and state variables including thermal pressurization are related by an equation analogous to Eq. 6:

$$f_{ss}^{TP}(V,\phi) = a \text{ arsinh}\left(\frac{V}{2V_0}\exp\frac{\Psi_{ss}^{TP}(V,\phi)}{a}\right) \tag{16}$$

Equating Eq. 14 with Eq. 16, we obtain an expression for $\Psi_{ss}^{TP}(V,\phi)$, which we use in the state evolution law as

$$\dot{\Psi} = -\frac{V}{L}(\Psi - \Psi_{ss}^{TP}(V,\phi)) \tag{17}$$

To include flash heating, we replace in Eq. 14 f_{ss} by ${f_{ss}}^{FH}$ as:

$$f_{ss}^{FH+TP} = \frac{f_{ss}^{FH}(V)}{(1+\frac{\phi}{L^*})^{1/3}} \tag{18}$$

We equate that with

$$f_{ss}^{FH+TP} = a \text{ arsinh}\left(\frac{V}{2V_0}\exp\frac{\Psi_{ss}^{FH+TP}}{a}\right) \tag{19}$$

to obtain Ψ_{ss}^{FH+TP}, which we then use in the state evolution law:

$$\dot{\Psi} = -\frac{V}{L}(\Psi - \Psi_{ss}^{FH+TP}) \tag{20}$$

The computational cost of the combined flash-heating and thermal pressurization model is comparable to that of a classical rate-and-state fault model.

3 Sample simulation results

We implemented the TP proxy and flash heating in the fully-dynamic 2.5D earthquake cycle simulation software SEM2DPACK based on the spectral element method (Ampuero, 2002; Kaneko et al., 2008, 2011; Liang et al., 2022). The 2.5D formulation is an approximation of the 3D problem accounting for the finite seismogenic width W (Weng and Ampuero, 2019, 2020; Liang et al., 2022). In Appendix 1 we calibrate the value of a geometric coefficient involved in the 2.5D model so that it produces results consistent with 3D dip-slip earthquake cycle simulations.

An example of the fault response in a 2.5D seismic cycle simulation is shown in Figure 2. Results are plotted during 5 cycles, starting at the second cycle to avoid effects of initial conditions. The simulation produces "characteristic earthquake" behavior: events spanning the whole fault occur regularly, with similar slip distribution and evolution along the fault (Figure 2a). The dependence of shear stress on slip follows the desired scaling $\tau \approx \delta^{-1/3}$ for each event (Figure 2b). The shear stress prior to each event is well below the peak friction coefficient, $\tau/\sigma \sim 0.3$ near the center of the fault (Figure 2c). As designed, the state variable ϕ mimics well the co-seismic slip of each event and resets to zero rapidly after each event (Figure 2d).

In Figure 3, we compare the dynamic response of a 2.5D fault with and without flash heating in addition to TP. We set equivalent initial conditions (Figure 3a) to compare the shear stress evolution as a function of slip (Figure 3b). For reference, we also show a model with only flash-heating (no TP) and a model with classical rate-and-state friction. For the latter, we had to set up a higher value of τ_0 to achieve a runaway rupture. As observed, only the models that account for TP exhibit a $\delta^{-1/3}$ decay of shear stress with slip. Although flash heating significantly reduces the shear strength (green curve in Figure 3b), it does not produce continued slip-weakening. When combining both mechanisms (magenta curve in Figure 3b), weakening at short slip is dominated by flash-heating first, while at large slip it is dominated by TP and leads to weakening $\propto \delta^{-1/3}$.

We further verify that our models of large earthquakes with TP are compatible with fracture mechanics theory. Large ruptures with rupture length $> W$ are pulse-like due to the 2.5D effect of the finite seismogenic width W (Figure 4a). When the rupture has propagated over distances significantly larger than W, the slip rate decays with distance behind the rupture front as $v \propto x^{-0.5}$ (red curve in Figure 4b), as expected from conventional singular pulse models. This result supports the use of fracture mechanics theory to understand the propagation and arrest of very large earthquakes, despite the continued weakening induced by TP. Only at propagation distances comparable to or shorter than W, the slip rate decays as $v \propto x^{-0.25}$ (blue curve in Figure 4b) which is the expected "unconventional singularity" for TP (Viesca and Garagash, 2015; Brener and Bouchbinder, 2021). At further distance in the tail of the pulse, the slip rate

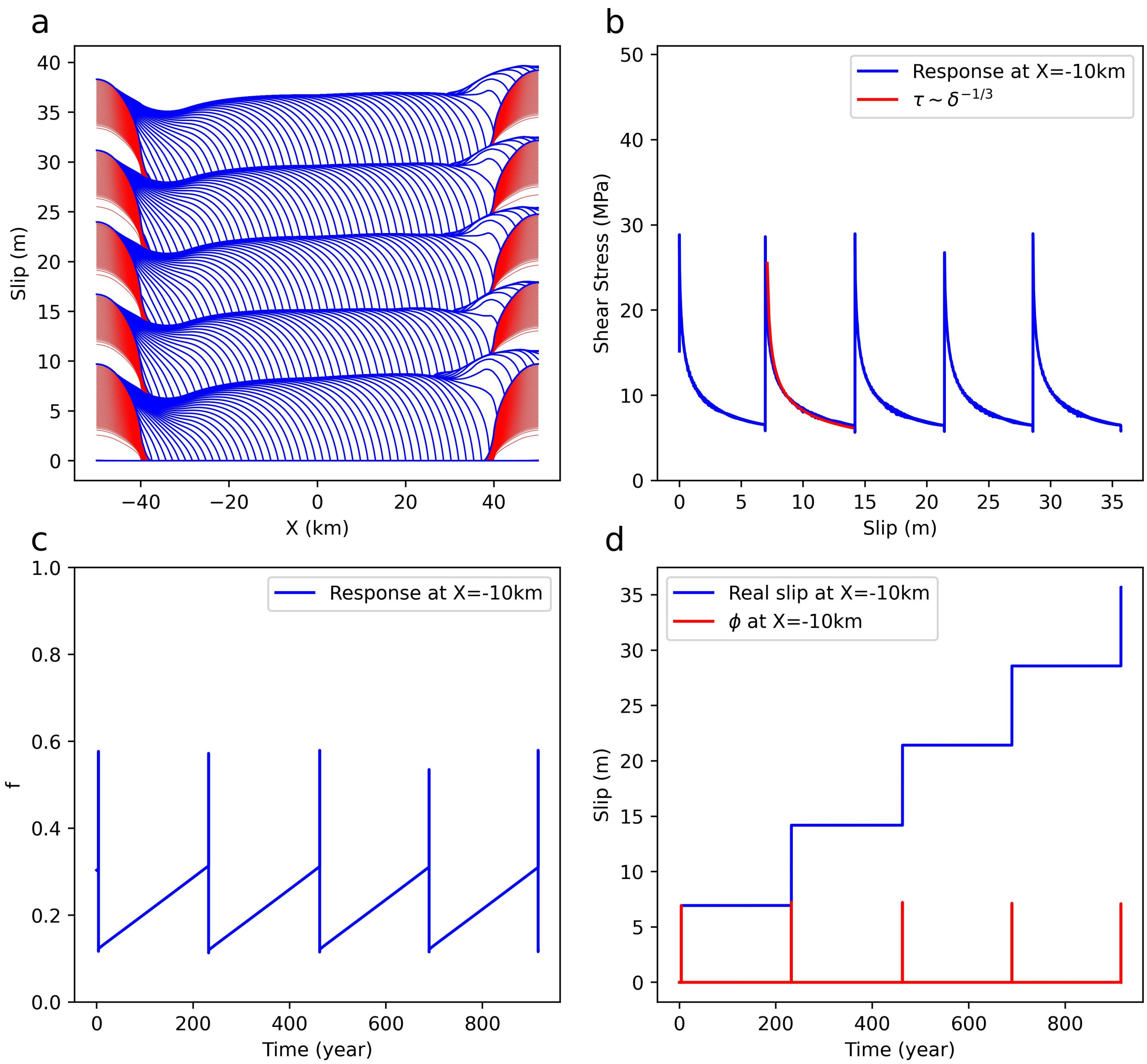

Figure 2: Results of a 2.5D earthquake cycle simulation on a homogeneous dip-slip shallow fault. Model parameters are $W = 20$ km, $\sigma = 50$ MPa, $L = 0.0075$ m, $L^* = 0.1$ m, $a_{VW} = 0.01$ and $b_{VW} = 0.015$. a) Slip evolution along the whole fault plotted every 0.5 s during seismic events (blue curves) and every 5 years in between earthquakes (red curves). At a representative point near the middle of the fault: b) shear-stress evolution as a function of slip, c) friction coefficient as a function of time, and d) temporal evolution of slip and TP state variable ϕ.

decays exponentially (Figure 4c), which is the expected behavior induced by the finite rupture width W in 2.5D models.

This is a non-peer reviewed preprint submitted to EarthArXiv and under review in Geophysical J.Int.

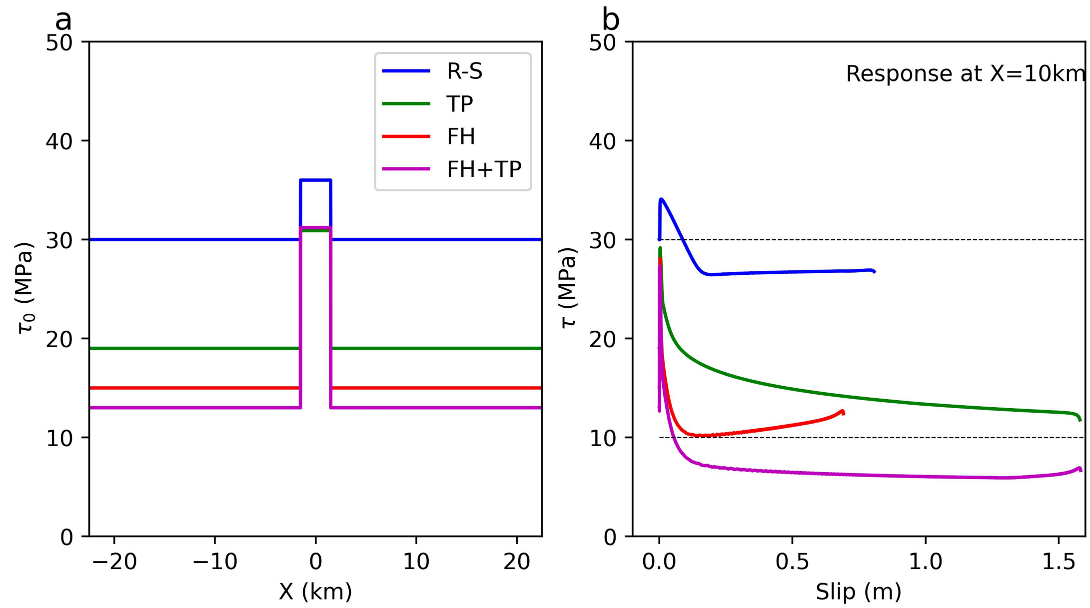

Figure 3: Dynamic response of a homogeneous dip-slip buried fault for cases with only rate-and-state friction (R-S), only thermal pressurization (TP), only flash heating (FH) and including both (FH+TP). Model parameters are $\sigma = 50$ MPa, $f_0 = 0.6$, $a = 0.0125$, $b = 0.0172$, $L = 0.015$ m, $L^* = 1$ m, $f_w = 0.2$ and $W = 10$ km. a) Initial shear stress. The nucleation patch is located at the center of the fault. b) Shear stress as a function of slip at a point located at 10 km from the nucleation patch.

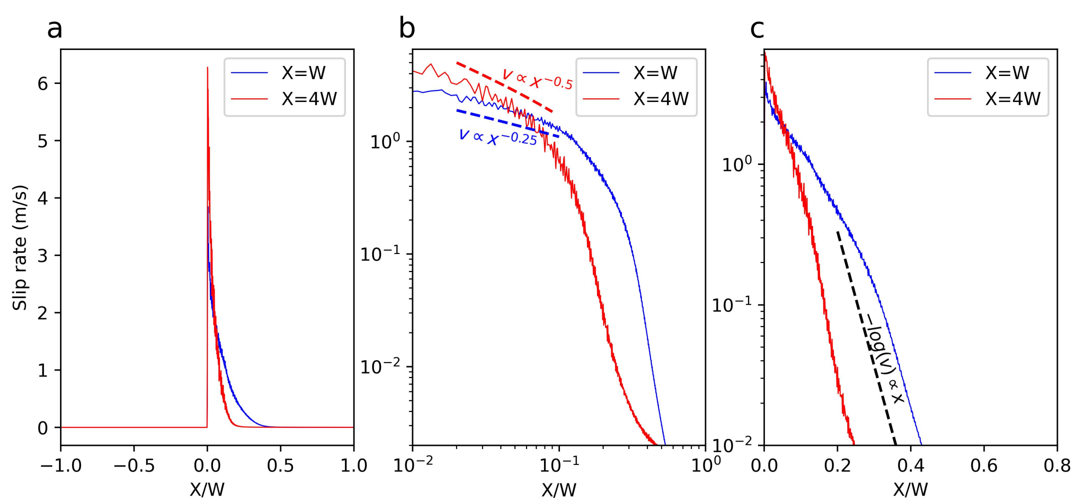

Figure 4: Spatial distribution of slip rate at two different times, when the rupture front has propagated up to positions $x = W$ and $x = 4W$. a) Slip rate as a function of distance, showing a pulse-like shape. The reference position ($x = 0$) is the location of the peak slip rate. b) Spatial decay of slip rate, with a focus on short distances from the rupture front. Unconventional $v \propto x^{-0.25}$ and conventional $v \propto x^{-0.5}$ asymptotic behaviors appear at small ($x = W$) and large ($x = 4W$) propagation distances, respectively. c) Exponential decay of slip rate at larger distances behind the rupture front, $\log(v) \propto -x$.

4 Fracture energy of the TP proxy

Our approach is designed to emulate the fault weakening and the relationship between fracture energy (G_c) and slip (δ) resulting from TP, focusing on large earthquakes with slips larger than 1 m. A different decay regime at short slip, $G_c \propto \delta^2$ (Viesca and Garagash, 2015), could be similarly introduced in the model by modifying Eq. 14.

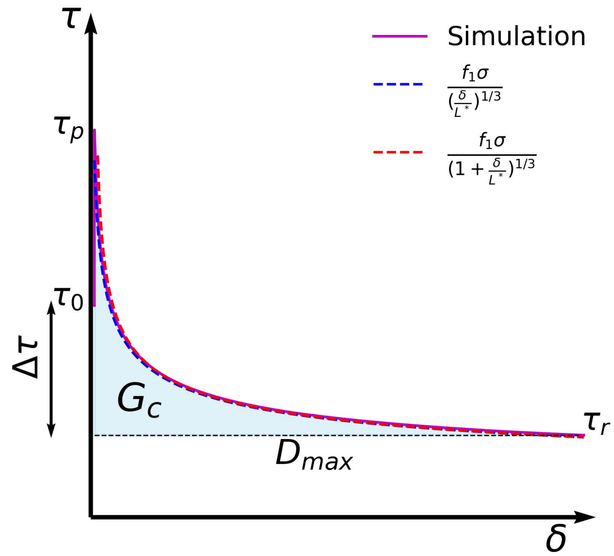

Figure 5: Fracture energy G_c prediction on rate-and-state faults with thermal pressurization proxy

To estimate G_c, we consider an earthquake with level of stress right before the nucleation, τ_0, and residual stress when the slip stops, τ_r. As we include a slip dependence on the steady state friction, the shear stress during an earthquake is a function of slip δ (Figure 5):

$$\tau(\delta) \approx \frac{f_1\sigma}{(1+\frac{\delta}{L^*})^{1/3}} \tag{21}$$

where σ is the effective normal stress on the fault, and f_1 a reduced reference friction coefficient that accounts for the early dependence of τ on velocity. Numerical results show that for $f_0 = 0.6$ and typical co-seismic velocities in the range of 1-20 m/s, $f_1 \approx 0.51 - 0.53$. The logarithmic dependence on velocity does not produce a significant reduction of the steady-state friction. When including flash heating, $f_1 \approx f_w$. Then, for maximum slip D:

$$\tau_r \approx \frac{f_1 \sigma}{(1 + \frac{D}{L^*})^{1/3}} \tag{22}$$

Following the definition of fracture energy:

$$G_c = \int_0^D [\tau(\delta) - \tau_r] \, d\delta \tag{23}$$

Solving the integral we get:

$$G_c \approx \left\{ 1.5L^* \left[\left(1 + \frac{D}{L^*}\right)^{2/3} - 1 \right] - \frac{D}{(1 + \frac{D}{L^*})^{1/3}} \right\} f_1 \sigma \tag{24}$$

This expression gives an accurate estimation of the fracture energy G_c.

For large slips, $D/L^* \gg 1$, we approximate $\tau(\delta)$ as:

$$\tau(\delta) \approx \frac{f_1 \sigma}{(\frac{\delta}{L^*})^{1/3}} \tag{25}$$

As shown in Figure 5, this gives an accurate approximation of the shear stress evolution. Then, using Eqs. 23 and 25 we obtain a simpler expression for the fracture energy:

$$G_c = 0.5 {L^*}^{1/3} D^{2/3} f_1 \sigma \tag{26}$$

This highlights the scaling $G_c \propto D^{2/3}$, similar to that in Viesca and Garagash (2015).

To evaluate the performance of both expressions (Eqs. 26 and 24) we plot in Figure 6 different values of G_c calculated from 2.5D dynamic simulations, both estimates and the estimate $G_c \approx (12\pi)^{-1/3} f_w \sigma D^{2/3} {L^*}^{1/3}$ by Viesca and Garagash (2015). As observed in Figure 6, Eq. 26 predicts accurately G_c for slips larger than 1 m. Comparing Figures 6a and 6b shows that the approximation improves at shorter values of L^*.

This is a non-peer reviewed preprint submitted to EarthArXiv and under review in Geophysical J.Int.

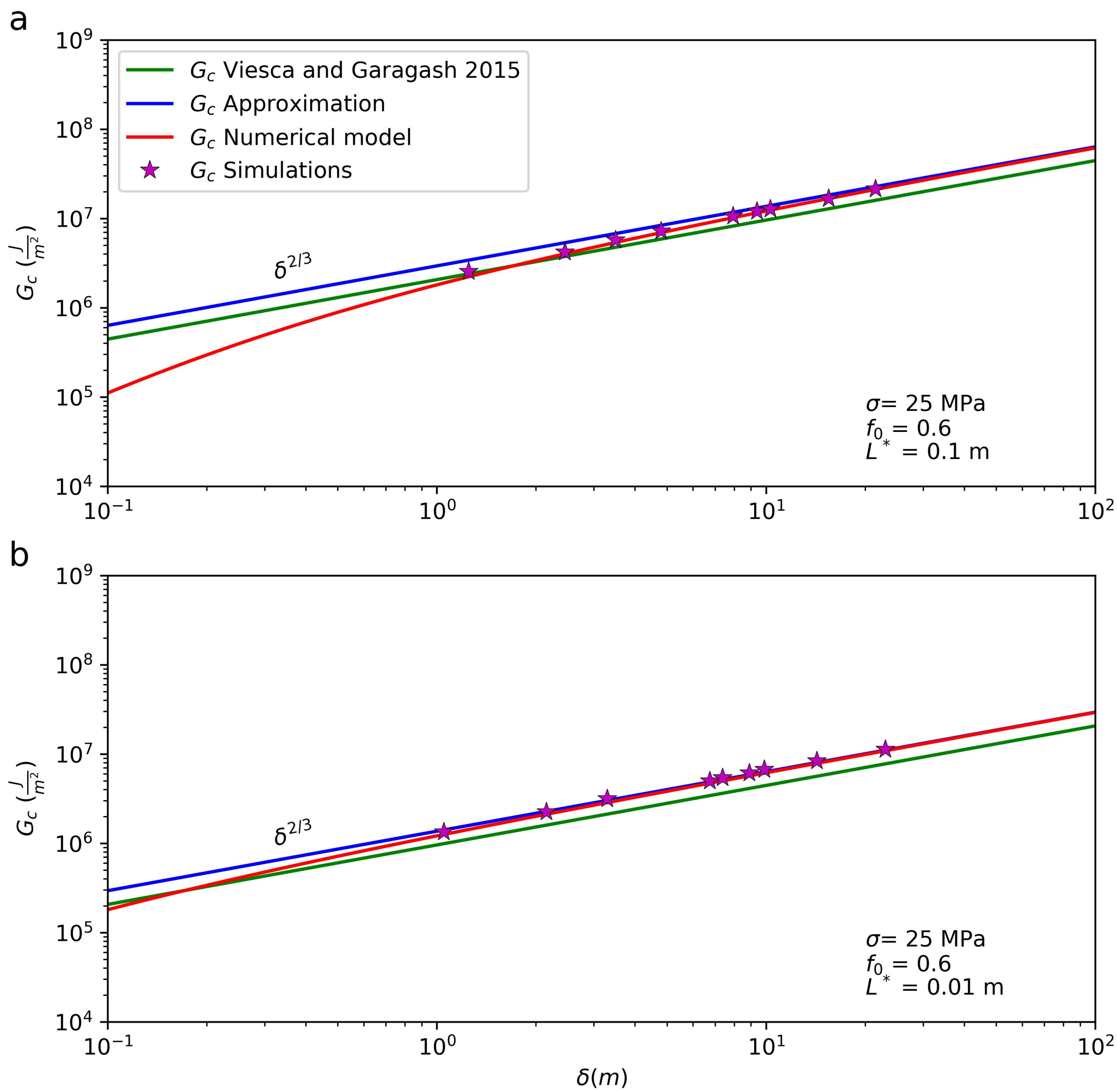

Figure 6: G_c prediction on 2.5D models for a) $L^* = 0.1$ m b) L^*= 0.01 m

5 Discussion and Conclusions

We have introduced a proxy for thermal pressurization implemented through a modified rate-and-state friction law. This approach is designed to emulate the fault weakening and the relationship between fracture energy and slip resulting from thermal pressurization. Compared to the classical rate-and-state model, an additional state variable is introduced and one additional state evolution equation is solved, whose calculation time is negligible. Therefore, the additional complexity and computational cost are negligible, unlike complete implementations of thermal pressurization that require solving fluid pressure and thermal diffusion equations.

Although here we demonstrate the concept in a 2.5D earthquake simulator based on the spectral element method, the thermal pressurization proxy only involves modifications of the friction solver, thus it can be readily implemented in 1D, 2D and 3D, and in simulators based on other numerical methods such as the finite element method and the boundary element method.

Moreover, it is possible to reproduce different decay laws of shear stress with slip, such as the undrained-adiabatic regime of thermal pressurization that could be dominant at shorter slip (Viesca and Garagash, 2015), by modifying Eq. 14.

Our proxy encapsulates the effects of thermal pressurization in a single parameter, the length scale L^* defined in equation 15. It depends on the fault zone physical parameters involved in the thermal and hydraulic diffusion equations. Varying L^*, earthquake models can be tuned between strong and weak thermal pressurization effects, or account for both cases on the same fault through spatial variations of L^* (Noda and Lapusta, 2013).

Carrying 2.5D simulations of large earthquakes, we find that, despite the continued slip-weakening behind the rupture front produced by thermal pressurization, the asymptotic behavior of slip rate is consistent with the conventional singularity of fracture mechanics theory, as soon as the rupture has propagated a distance larger than the rupture width. This result supports the applicability of fracture mechanics theory to understand the propagation and arrest of large earthquakes. We derive and validate theoretical predictors of fracture energy G_c (Eq. 26) in earthquake cycle models, which can be used to evaluate the rupture potential of fault segments (Weng and Ampuero, 2019, 2020). These results can have important implications for understanding earthquake mechanics.

Acknowledgments

M.H. acknowledges the support by ANID "Agencia Nacional de Investigación y Desarrollo Subdirección de Capital Humano/Doctorado Nacional/2020" national Ph.D. scholarship 21201352. J.P.A. was supported by the French government through the UCAJEDI Investments in the Future project (ANR-15-IDEX-01) managed by the National Research Agency (ANR). The authors are grateful to the OPAL infrastructure and the Université Côte d'Azur's Center for High-Performance Computing for providing resources and support. M.H. and J.G.F.C. acknowledge the funding support by ANID/FONDAP/15110017 (Centro de Investigación para la Gestión Integrada del Riesgo de Desastres [CIGIDEN]). J.G.F.C. acknowledges support from ANID/FONDECYT/11201180 (Dynamic Rupture on Faults with Heterogeneous Frictional Properties).

Author contribution statement

J.P.A. developed the conceptual idea of the study. M.H. and J.P.A. developed the analytical validations. M.H conducted the code implementation, numerical validations and wrote the original manuscript draft. M.H., J.P.A. and J.G.F.C. contributed to the writing and review process. J.P.A. and J.G.F.C. supervised the work.

Open Research

The code employed in this research is SEM2DPACK. This is an open access spectral element method code, available to download in https://github.com/jpampuero/sem2dpack.

References

Abercrombie, R. E. and Rice, J. R. (2005). Can observations of earthquake scaling constrain slip weakening? *Geophysical Journal International*, 162:406–424.

Aki (1966). Generation and propagation of G-waves from the Niigata earthquake of June 16, 1964, 2. Estimation of earthquake moment, released energy, and stress-strain drop from G-wave spectrum. *Earthquake Res. Inst.*, 44:73–88.

Ampuero, J.-P. (2002). *Étude physique et numérique de la nucléation des séismes*. PhD thesis, University of Paris VII. Thèse de doctorat dirigée par Vilotte, Jean-Pierre Géophysique interne Paris 7 2002.

Andrews, D. J. (1976). Rupture propagation with finite stress in antiplane strain. *Geophysical Research Letters*, 81:3575–3582.

Beeler, N. M., Tullis, T. E., and Goldsby, D. L. (2008). Constitutive relationships and physical basis of fault strength due to flash heating. *Journal of Geophysical Research*, 113.

Ben-Zion, Y. and Rice, J. R. (1997). Dynamic simulations of slip on a smooth fault in an elastic solid. *J. Geophys. Res.*, 102(17):771784.

Brener, E. and Bouchbinder, E. (2021). Unconventional singularities and energy balance in frictional rupture. *Nature Communications*.

Dieterich, J. (1978). Time-dependent friction and the mechanics of stick-slip. *Pure and Applied Geophysics*, 116(4):790–806.

Dieterich, J. (1979). Modeling of rock friction: 1. experimental results and constitutive equations. *Journal of Geophysical Research: Solid Earth*, 84:2161–2168.

Garagash, D. I. (2012). Seismic and aseismic slip pulses driven by thermal pressurization of pore fluid. *Journal of Geophysical Research*, 117.

Goldsby, D. L. and Tullis, T. E. (2011). Flash heating leads to low frictional strength of crustal rocks at earthquake slip rates. *Science*, 334:216–218.

Harris, R. A., Barall, M., Archuleta, R., Dunham, E., Aagaard, B., Ampuero, J. P., Bhat, H., Cruz-Atienza, V., Dalguer, L., Dawson, P., Day, S., Duan, B., Ely, G., Kaneko, Y., Kase, Y., Lapusta, N., Liu, Y., Ma, S., Oglesby, D., Olsen, K., Pitarka, A., Song, S., and Templeton, E. (2018). A Suite of Exercises for Verifying Dynamic Earthquake Rupture Codes. *Seismological Research Letters*, 89(3):1146–1162.

Ida, Y. (1972). Cohesive force across the tip of a longitudinal-shear crack and Griffith's specific surface energy. *Journal of Geophysical Research: Solid Earth*, 77:3796–3805.

Kanamori, H. and Anderson, D. (1975). Theoretical Basis of Some Empirical Relations in Seismology. *Bulletin of the Seismological Society of America*, 65:1073–1095.

Kaneko, Y., Ampuero, J.-P., and Lapusta, N. (2011). Spectral-element simulations of long-term fault slip: Effect of low-rigidity layers on earthquake-cycle dynamics. *Journal of Geophysical Research: Solid Earth*, 116.

Kaneko, Y., Lapusta, N., and Ampuero, J.-P. (2008). Spectral element modeling of spontaneous earthquake rupture on rate and state faults: Effect of velocity-strengthening friction at shallow depths. *Journal of Geophysical Research*, 113.

Lambert, V. and Lapusta, N. (2023). Absolute stress levels in models of low-heat faults: Links to geophysical observables and differences for crack-like ruptures and self-healing pulses. *Earth and Planetary Science Letters*, 618:118277.

Lapusta, N., Rice, J., Ben-Zion, Y., and Zheng, G. (2000). Elastodynamic analysis for slow tectonic loading with spontaneous rupture episodes on faults with rate-and state-dependent friction. *Journal of Geophysical Research: Solid Earth*, 105.

Liang, C., Ampuero, J.-P., and Muñoz, D. (2022). The paucity of supershear earthquakes on large faults governed by rate and state friction. *Geophysical Research Letters*, 49.

Luo, Y., Ampuero, J. P., Galvez, P., van den Ende, M., and Idini, B. (2017). *QDYN: a Quasi-DYNamic earthquake simulator (v1.1)*. Zenodo.

Mase, C. W. and Smith, L. (1987). Effects of frictional heating on the thermal, hydrologic, and mechanical response of a fault. *Journal of Geophysical Research*, 92:6249–6272.

Mavrommatis, A. P., Segall, P., and Johnson, K. (2017). A physical model for interseismic erosion of locked fault asperities. *Journal of Geophysical Research: Solid Earth*, 122:8326–8346.

Noda, H. and Lapusta, N. (2013). Stable creeping fault segments can become destructive as a result of dynamic weakening. *Nature*, 493:518–521.

Noda, H., Lapusta, N., and Rice, J. (2011). Earthquake sequence calculations with dynamic weakening mechanisms. *Springer Series in Geomechanics and Geoengineering*, 113:149–152.

Perry, S., Lambert, V., and Lapusta, N. (2020). Nearly magnitude-invariant stress drops in simulated crack-like earthquake sequences on rate-and-state faults with thermal pressurization of pore fluids. *Journal of Geophysical Research: Solid Earth*, 125.

Rempel, A. W. and Rice, J. R. (2006). Thermal pressurization and onset of melting in fault zones. *Journal of Geophysical Research*, 111.

Rice, J. and Ruina, L. (1983). Stability of Steady Frictional Slipping. *J. Appl. Mech.*, 50(2):343–349.

Rice, J. R. (2006). Heating and weakening of faults during earthquake slip. *Journal of Geophysical Research*, 111.

Ruina (1983). Slip instabilities and state variable friction laws. *J. Geophys. Res.*, 88(10):359–370.

Starr, A. (1928). Slip in a crystal and rupture in a solid due to shear. *Proc. Cambridge Phil. Sop.*, 24:489–500.

Thomas, M. Y., Lapusta, N., and Avouac, J.-P. (2014). Quasi-dynamic versus fully dynamic simulations of earthquakes and aseismic slip with and without enhanced coseismic weakening. *Journal of Geophysical Research Solid Earth*, 119:1986–2004.

Tinti, E., Spudich, P., and Cocco, M. (2005). Earthquake fracture energy inferred from kinematic rupture models on extended faults. *Journal of Geophysical Research*, 110.

Viesca, R. and Garagash, D. (2015). Ubiquitous weakening of faults due to thermal pressurization. *Nature Geoscience*, 8(11):875–879.

Weng, H. and Ampuero, J.-P. (2019). The dynamics of elongated earthquake ruptures. *Journal of Geophysical Research: Solid Earth*, 124(8):8584–8610.

Weng, H. and Ampuero, J.-P. (2020). Continuum of earthquake rupture speeds enabled by oblique slip. *Nature Geoscience*, 13:817–821.

Appendices

A Calibration of the 2.5D model

The slip in 2.5D models corresponds to the peak slip across the seismogenic depth of a 3D model. The slip on a deeply buried fault with uniform stress drop can be crudely approximated as one half of a cosine of wavelength 2W. Similarly, in a shallow fault on a half-space, the slip is maximal at the surface and zero at the bottom of the rupture, and the depth profile can be approximated as one quarter of a cosine of wavelength $4W$ (Weng and Ampuero, 2019). However, as these approximations are crude, the $W_{2.5D}$ used in the 2.5D code might differ from an equivalent W_{3D}. Here we determine the relation between $W_{2.5D}$ and W_{3D}.

For the 3D model, a theoretical relation between stress drop $\Delta\tau$ and slip is (Kanamori and Anderson, 1975):

$$\Delta\tau = C\mu\frac{\bar{\delta}}{\bar{L}} \tag{A.1}$$

This is a non-peer reviewed preprint submitted to EarthArXiv and under review in Geophysical J.Int.

For a shallow infinitely long dip-slip fault, $\bar{L} = W$ (width) and:

$$C = \frac{4(\lambda + \mu)}{\pi(\lambda + 2\mu)} \tag{A.2}$$

where λ is the Lamé constant (Aki, 1966; Starr, 1928). Then, we obtain:

$$\frac{\Delta\tau}{\bar{\delta}} = \frac{\frac{4(\lambda+\mu)}{\pi(\lambda+2\mu)}\mu}{W_{3D}} \tag{A.3}$$

From Figure 1 of Kanamori and Anderson (1975), noting that average slip $\bar{\delta}$ and peak slip D_{max} in a crack are related by $\bar{\delta} = \frac{\pi}{4}D_{max}$:

$$\frac{\Delta\tau}{D_{max}} = \frac{\frac{(\lambda+\mu)}{(\lambda+2\mu)}\mu}{W_{3D}} \tag{A.4}$$

Replacing $\lambda = \frac{2\mu\nu}{1-2\nu}$ we get:

$$D_{max} = \frac{2(1-\nu)\Delta\tau W_{3D}}{\mu} \tag{A.5}$$

For the 2.5D model without free-surface effect:

$$D = \frac{\Delta\tau W_{2.5D}}{\pi\mu} \tag{A.6}$$

As D in the 2.5D model corresponds to D_{max} in a 3D equivalent model with similar $\Delta\tau$, equating Eqs. A.5 and A.6 gives:

$$W_{2.5D} = 2\pi(1-\nu)W_{3D} \tag{A.7}$$

For $\nu = 1/4$, we must set $W_{2.5D} = 4.71\,W_{3D}$ to obtain an equivalent model for a shallow fault. For a buried fault, following a similar procedure we obtain $W_{2.5D} = 2.36\,W_{3D}$. Both values were validated numerically (see Figure A.1.) by comparing 3D simulations with 2.5D simulations using the quasi-dynamic boundary element method simulator QDYN (Luo et al., 2017).

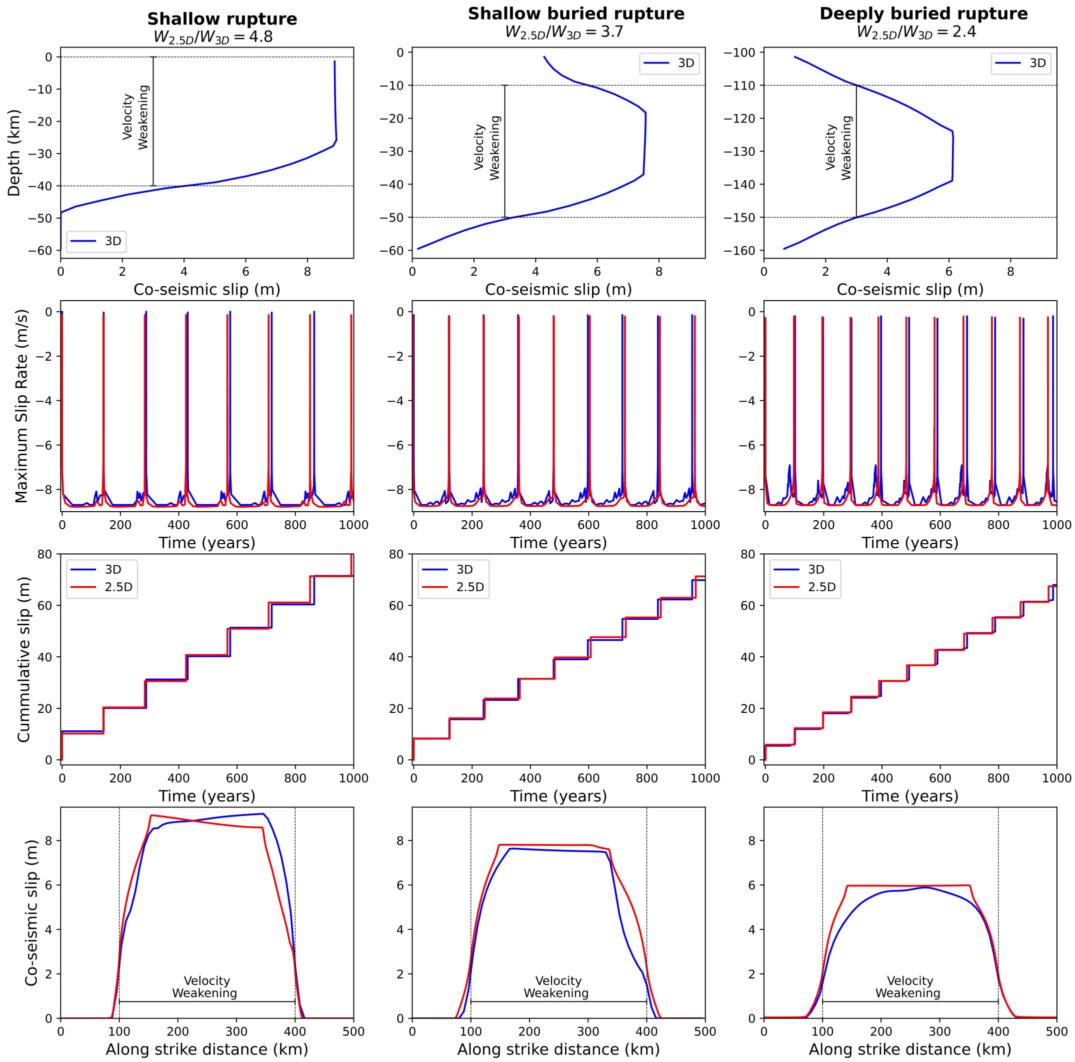

Figure A.1: Quasi-dynamic W calibration for 2.5D and 3D models. a) Shallow fault. b) Slightly buried fault. c) Deeply buried fault.

B Tables

Parameter	Symbol	Value
Shear modulus	μ	32 GPa
Shear wave speed	V_s	3464 m/s
Reference friction coefficient	f_0	0.6
Reference slip rate	V_0	10^{-6} m/s
Loading plate velocity	V_{PL}	10^{-9} m/s

Table B.1: Parameters used in this study